ACS ORGANIC & INORGANIC Au
AN OPEN ACCESS JOURNAL OF THE AMERICAN CHEMICAL SOCIETY

Open Access
This article is licensed under CC-BY-NC-ND 4.0

pubs.acs.org/orginorgau
Article

# Copper-Mediated −CF(OCF$_3$)(CF$_2$H) Transfer to Organic Electrophiles

Behnaz Ghaffari,[‖] Luana L. T. N. Porto,[‖] Nicole Johnson, Jeffrey S. Ovens, Christian Ehm,* and R. Tom Baker*

Cite This: ACS Org. Inorg. Au 2024, 4, 628−639
Read Online
ACCESS | Metrics & More | Article Recommendations | Supporting Information

**ABSTRACT:** The integration of fluorine into medicinal compounds has become a widely used strategy to improve the biochemical and therapeutic properties of drugs. Inclusion of −CF$_2$H and −OCF$_3$ fluoroalkyl groups has garnered attention due to their bioisosteric properties, enhanced lipophilicity, and potential hydrogen-bonding capability in bioactive substances. In this study, we prepared a series of stable Cu[CF(OCF$_3$)(CF$_2$H)]L$_n$ complexes by insertion of commercially available perfluoro(methyl vinyl ether), CF$_2$═CF(OCF$_3$), into Cu−H bonds derived from Stryker's reagent, [CuH(PPh$_3$)]$_6$, using ancillary ligands L. Notably, certain of these complexes effectively transfer the fluoroalkyl group to aroyl chlorides. Through reaction optimization and computational analysis, we identified dimethylsulfoxide as a pivotal coligand, playing a distinctive role in enabling the fluoroalkylation of a range of aroyl chlorides and aryl iodides. The latter also benefits from addition of CuBr to abstract PPh$_3$, generating solvent-stabilized Cu[CF(OCF$_3$)(CF$_2$H)]. These methodologies allow for the introduction of geminal −OCF$_3$ and −CF$_2$H groups in a single transformation.

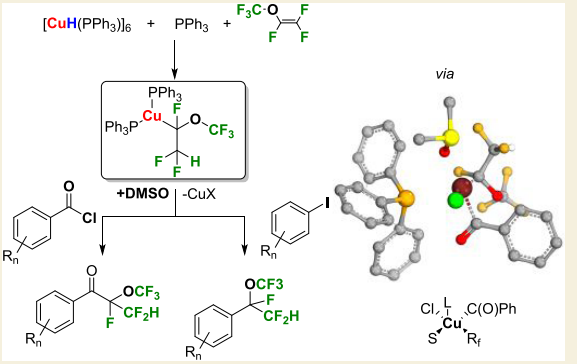


**KEYWORDS:** *copper-mediated fluoroalkylation, fluoroketones, fluorinated aromatics, difluoromethyl, trifluoromethoxy*

## INTRODUCTION

The success of organofluorine compounds in the pharmaceutical[1] and agrochemical[2] markets has inspired researchers to develop more efficient late-stage fluorination[3,4] and fluoroalkylation protocols.[5,6] While there are many methodologies to incorporate the trifluoromethyl group into organic substrates,[7−9] fewer examples have been reported for other fluoroalkyl groups such as −C$_2$F$_5$,[10−12] −OCF$_3$,[13−15] and −CF$_2$H.[16−18] Nonetheless, such functional groups have already appeared in useful drugs: *cf.* −OCF$_3$ in Riluzole (glutamate antagonist used as an anticonvulsant)[19] and Triflumuron (pesticide)[20] and −CF$_2$H in PQR620 (mTOR inhibitor, anticancer)[21] and Pantoprazole (proton pump inhibitor; Figure 1).[22]

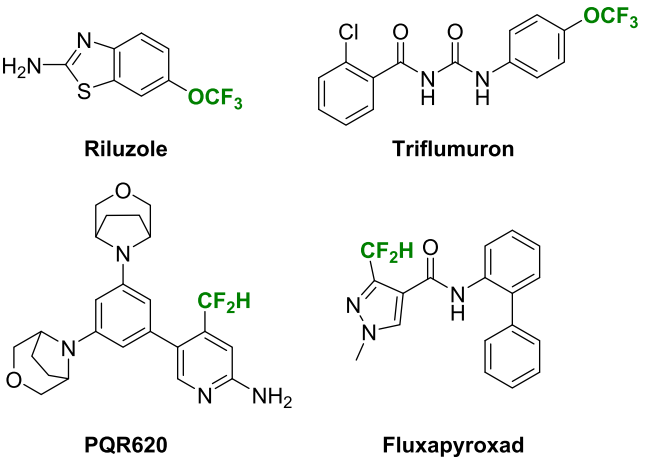


**Figure 1.** Bioactive compounds containing −OCF$_3$ and −CF$_2$H groups.

Increased interest in these two substituents results from their biosteric properties. In contrast to the OCH$_3$ group in anisole, the OCF$_3$ group is not coplanar with its attached aryl ring, and adjacent $\sigma$ bonds can interact with the low-energy $\sigma^*$ orbital of the O−C$_{CF3}$ bond.[23] The −CF$_2$H group has been intensively studied over the past few years due to its unique properties, such as Brønsted acidity and ability to act as a hydrogen-bond donor while still modulating lipophilicity.[24] Moreover, its small steric signature allows it to adopt an optimal conformation based on specific drug targets.[25,26] Bulkier R$_f$ groups such as perfluoroisopropyl have also imparted unique activity in several agrochemicals.[27,28]

Chelating nitrogen ligands have been shown previously to promote Cu-mediated fluoroalkyl transfer to organic electro-

Received: June 1, 2024
Revised: August 15, 2024
Accepted: August 26, 2024
Published: September 20, 2024

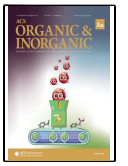

© 2024 The Authors. Published by American Chemical Society

**Scheme 1. Synthesis of $Cu[CF(OCF_3)CF_2H](PPh_3)_2$ (1)**

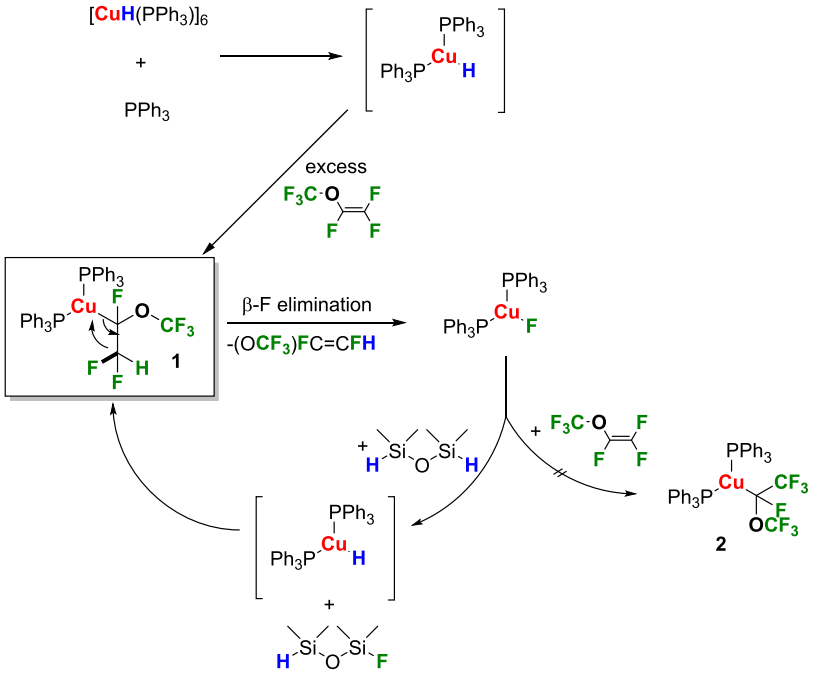


philes.[29−33] We recently reported the fluoroalkylation of aroyl chlorides with a phenanthroline copper heptafluoroisopropyl complex, [Cu(hfip)($PPh_3$)(phen)].[33] Although inclusion of phen was crucial for successful fluoroalkylation, stabilization of the hfip group was initially achieved by inserting hexafluoropropene (HFP) into the Cu-F bond of $CuF(PPh_3)_3$.[34] However, attempts to transfer the hfip group to aryl iodides were unsuccessful.

In this work, we employ commercially available perfluoro(methyl vinyl ether) [PMVE, $CF_2$═$CF(OCF_3)$], in the synthesis of new copper fluoroalkyls $Cu[CF(OCF_3)(CF_2H)]L_n$ that contain geminal $-OCF_3$ and $-CF_2H$ groups, offering a bulky $R_f$ group that includes a hydrogen-bond donor. We also demonstrate, both experimentally and computationally, the privileged role of the dimethylsulfoxide coligand in enabling fluoroalkylation of a range of aroyl chlorides and aryl iodides. The latter reaction is additionally facilitated by the use of CuBr to sequester the $PPh_3$ ligands, affording the more active solvent-stabilized 'Cu-$R_f$' transfer agent.

## RESULTS AND DISCUSSION

### Synthesis and Characterization of $Cu[CF(OCF_3)(CF_2H)]L_n$

Reaction of 5 equiv of PMVE with a mixture of $[CuH(PPh_3)]_6$, $PPh_3$ (2 equiv per Cu) and tetramethyldisiloxane (TMDSO) (1.5 equiv) gave a yellow solution of $Cu[CF(OCF_3)(CF_2H)](PPh_3)_2$ (**1**) from which colorless crystals could be isolated in 90% yield. Addition of the Si-H-containing siloxane converted any Cu-F (byproduct of $\beta$-F elimination) back to Cu-H to avoid formation of the $Cu[CF(OCF_3)(CF_3)]$ complex (**2**; Scheme 1). Similar reactions using alkyl phosphine ligands did not selectively afford the desired product, generating P−F bonds and additional uncharacterized side-products. The molecular structure of **1** shows a distorted trigonal-planar copper with a P-Cu-P angle of 114.5° and P-Cu-C angles of 126.6 and 118.5° (Figure 2). The Cu-C bond distance (2.062 Å) is longer than that observed in Cu-hfip (2.003 Å)[33] and Cu-$CF_2CF_3$ complexes (1.99 Å),[30] presumably reflecting the influence of the bulky $OCF_3$ group.

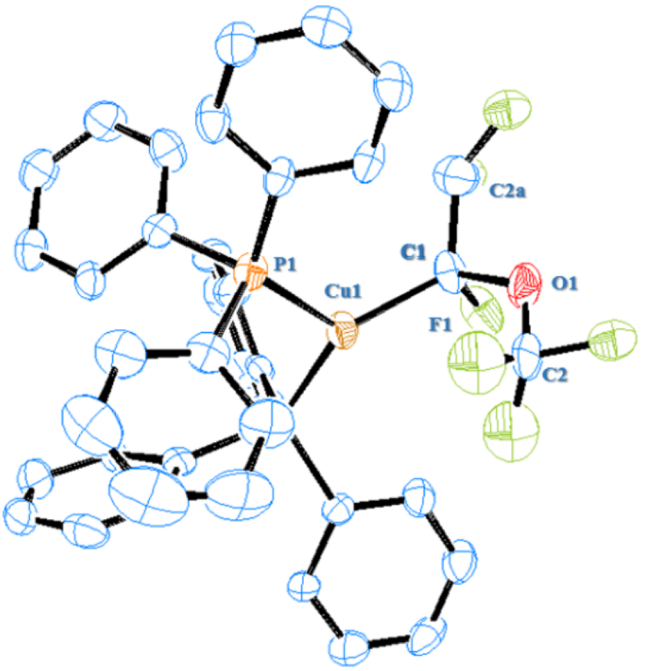


**Figure 2.** ORTEP representation of the molecular structure of **1**. Thermal ellipsoid probabilities are set at 35% and hydrogens atoms are omitted for clarity. Selected bond distances (Å) and angles (°): Cu-C1 2.062(16) Cu-P1 2.271(2) Cu-P2 2.286(2) C1-F1 1.42(2) C1-O1 1.48(1) C1-C2a 1.57(2) P1-Cu-C1 118.50(4) P1-Cu-P2 114.50(9) P2-Cu-C1 126.7(4).

### Reactivity of 1 with Aroyl Chlorides

Beginning with benzoyl chloride, addition of 1 equiv of **1** in a range of solvents (Table S1, entries 1−9) was monitored using $^{19}F$ NMR spectroscopy. In contrast to our previous results with transfer of the hfip group that required dimethylformamide


https://doi.org/10.1021/acsorginorgau.4c00038
ACS Org. Inorg. Au 2024, 4, 628−639

(DMF) solvent,[33] successful transfer of the 1-trifluoromethyl-1,2,2-trifluoromethoxy-ethyl (ttfet) group to give **3a** was only realized in dimethylsulfoxide (DMSO) solvent;[35] using **1** with other coordinating polar solvents led to decomposition of the Cu complex after 2 h. Moderate heating (40 °C) of the reactions in dry tetrahydrofuran (THF), toluene, diethyl ether ($Et_2O$) or hexane resulted in formation of hydrofluoroether $CHF(OCF_3)(CF_2H)$ (**4**) from the decomposition of **1**. After determining the optimal solvent, we next examined a limited aroyl chloride substrate scope. Monitoring the reactions by $^{19}F$ NMR showed that yields were limited by side-products derived from reaction of **1** with the DMSO solvent. Indeed, by conducting the $R_f$ transfer reactions in benzene with ca. 22 equiv of DMSO, yields after 2 h were now good to excellent for both electron-withdrawing (**3b**) and -donating (**3e**) aryl groups and sterically hindered products (Table 1).

**Table 1. Aroyl Chloride Fluoroalkylation Substrate Scope**[a]

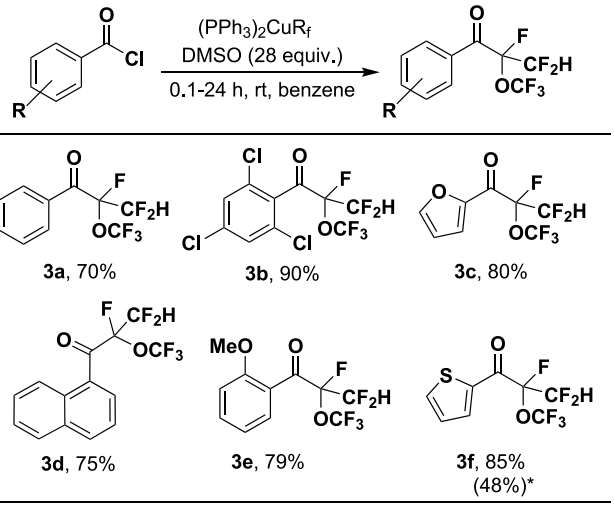


[a]Reactions conducted in an NMR tube; 0.03 mmol of **1** and aroyl chloride in $C_6D_6$/DMSO-$d_6$ (9:1). Yields determined by $^{19}F$ NMR; averages of at least duplicate experiments. * Conducted in DMSO.

Characterization of the fluoroalkylated ketone products **3a–f** showed large shifts for the C–F bond of the ttfet group in $^{19}F$ NMR (from −119.9 in **1** to ca. −81 ppm) and of the $CF_2H$ in $^1H$ NMR (from $\delta$ 5.62 in **1** to 5.9–6.9). Isolation and further characterization of **3a–f**, however, proved to be challenging due to their low boiling points and instability (see Supporting information (SI)). As a result, on a 0.3 mmol scale, **3d–f** were separated as benzene solutions using vacuum transfer. NMR analysis indicated decomposition to a single unidentified volatile product (no GC/MS peaks) with $R_f$ resonances ($CF_2H$ at $\delta$ 4.74) but none due to aryl rings. Moreover, $^{31}P$ NMR analysis of the reaction mixtures revealed the formation of $O{=}PPh_3$, suggesting that DMSO may be playing an additional role as oxidant in the reaction. Indeed, yellow crystals obtained from the reaction workup of **3e** in air turned out to be the previously reported[36] tetranuclear, oxo-bridged complex, $[CuCl(dmso)]_4(\mu_2\text{-}Cl)_4(\mu_4\text{-}O)$ (**5**) with four square pyramidal Cu(II) centers no longer coordinated to any $PPh_3$ ligands.

## Influence of Ancillary Ligands on Fluoroalkylation Efficiency

In light of previous reports using chelating nitrogen ligands in Cu-mediated fluoroalkyl transfer to organic electrophiles,[29−33] we embarked on the synthesis of a 1,10-phenanthroline (phen) analogue. Although the reaction product of **1** with phen (**6a**) could be characterized by NMR spectroscopy, formation of several byproducts hampered its full characterization, whereas reaction of **1** with 4,4′-dichloro-2,2′-bipyridine proceeded smoothly to afford 4-coordinate $Cu[CF(OCF_3)(CF_2H)](PPh_3)(bpy\text{-}Cl_2)$ (**6b**). Finally, reaction of **1** with the 7-Dipp NHC ligand gave 2-coordinated analogue **7** (Scheme 2; 7-Dipp = $:C[(dipp)N(CH_2)_2]_2$, dipp = 2,6-$^i$Pr$_2$C$_6$H$_3$). The molecular structure of **6b** (Figure 3A) exhibits a distorted tetrahedral geometry due to the acute N-Cu-N angle and a longer Cu-$C^F$ distance than that in three-coordinate **1**. The molecular structure of **7** features the ttfet group and the seven-membered ring NHC in a linear geometry, with shorter Cu-$C_\alpha$ and $C_\alpha$-F bond distances than those in **1** and **6b** (Figure 3B). Although complexes **6a,b** could not effect fluoroalkylation of benzoyl chloride in DMSO, complex **7** reacted completely, forming a mixture that did not include **3a** (see SI).

**Scheme 2. Synthesis of Additional Cu-ttfet Complexes (dipp = 2,6-$^i$Pr$_2$C$_6$H$_3$)**

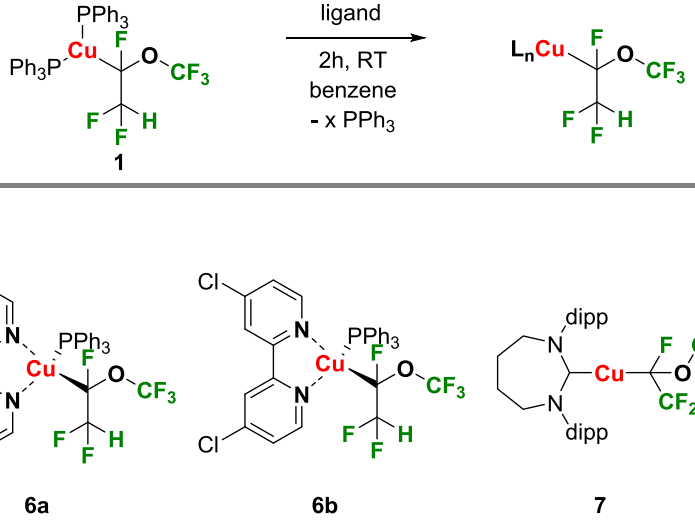




https://doi.org/10.1021/acsorginorgau.4c00038
ACS Org. Inorg. Au 2024, 4, 628–639

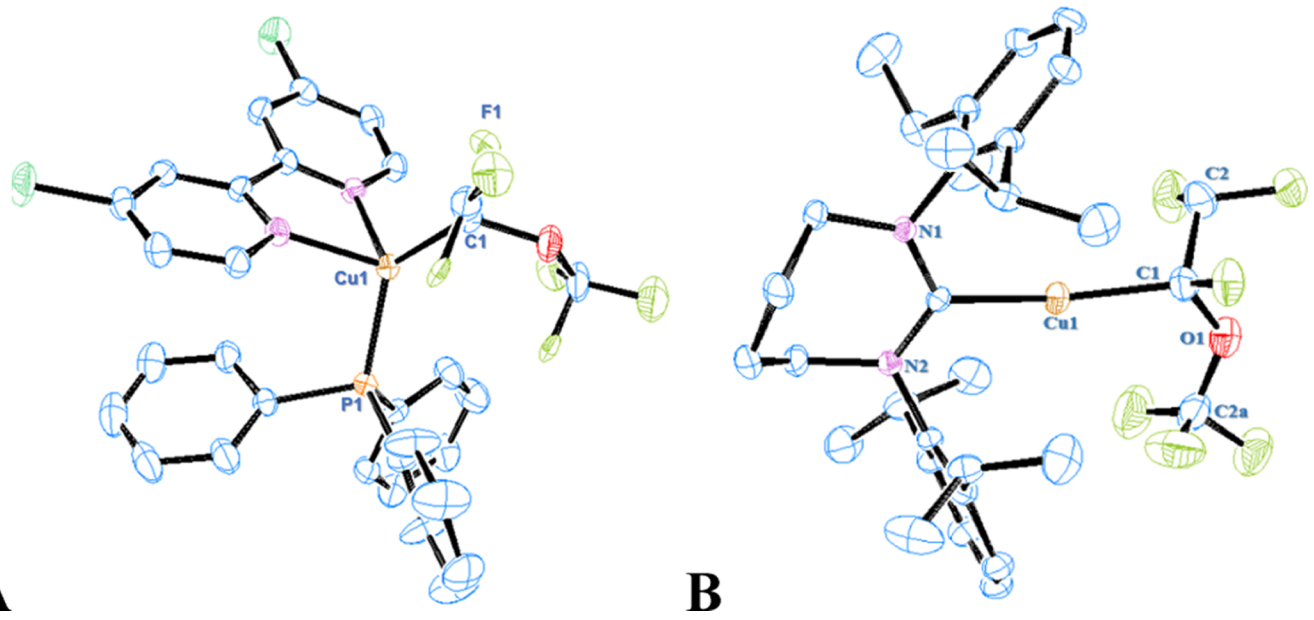


**Figure 3.** ORTEP representation of the molecular structures of **6b** (A) and **7** (B). Thermal ellipsoid probabilities are set to 35%, with hydrogen atoms omitted for clarity. Selected bond distances (Å) and angles (°) for **6b**: Cu-C 2.00(1) Cu-P 2.235(2) Cu-N1 2.105(9) Cu-N2 2.133(7) C1-F1 1.44(2) C1-Cu-P1 125.4(3) C1-Cu-N1 105.1(4) C1-Cu-N2 125.1(4) P1-Cu-N1 112.2(2) P1-Cu-N2 101.6(2) N1-Cu-N2 76.8(3) and for **7**: Cu-C1 1.975(5) Cu-C2 1.919(2) C1-F1 1.437(7) C1-Cu-C2 165.1(2).

## Fluoroalkylation of Aryl Iodides

In previous work, we were unable to transfer the hfip group from Cu(hfip)(phen)($PPh_3$) to aryl iodides.[33] Similarly, using **1** in DMSO led to its decomposition before any transfer could occur. Curiously, conducting the reaction in benzene solvent at 50 °C with just 8 equiv of DMSO, we observed some ttfet transfer to several electron-poor aryl iodides. Increasing the concentration beyond 8 equiv led to more decomposition of complex **1** (see SI). In his work on pentafluoroethylation, Hartwig reported that less electron-donating bpy ligands increased the rate of $R_f$ transfer from Cu to aryl chlorides.[37] Indeed, heating **6b** with electron-poor aryl iodides at 85 °C in toluene provided a second example of successful transfer of the ttfet group. However, yields were limited due to poor selectivity.

Given these first results with DMSO and bpy-$Cl_2$, we sought to optimize the fluoroalkylation of aryl halides. Inspired by previous work by Grushin et al.[38] and Boutureira and co-workers,[39,40] we aimed to access a polar solvent-stabilized, "ligandless" Cu(ttfet) complex by using Cu halide salts, CuX, to trap the $PPh_3$ ligands of **1**. To avoid decomposition of **1**, we used a minor amount of coordinating solvent to stabilize the copper salt in benzene, followed by precipitation of CuX-($PPh_3$)$_2$. The $ArR_f$ (**8a**) yield decreased to less than 5% when DMF was used as cosolvent (Table 2, entries 4, 8, and 12). Further screening of different CuX confirmed that CuBr was the most efficient copper salt, producing **8a** in 82% when used with a 2:1:1 ratio of CuBr/substrate/**1** (entry 11). Next, to optimize the DMSO concentration, we conducted experiments under our best conditions (Table 2, entry 11) with the less reactive substrate, 4-iodoanisole (Figure S1), which showed that 25 equiv of DMSO gave the highest yield (Figure S1). The reaction time course for iodobenzonitrile demonstrated fast oxidative addition in the first 10 min, slowing down every 10 min thereafter (see SI).

**Table 2. Optimization of the Preparation of "Ligandless" "Cu[$CF(OCF_3)CF_2H$]"**[a]

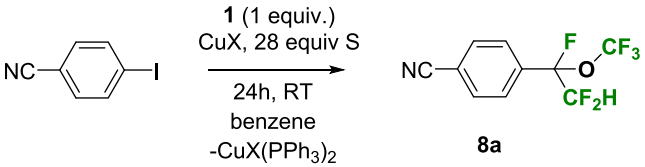


| entry | CuX | CuX (equiv) | substrate (equiv) | solvent (S) | yield (%) |
|---|---|---|---|---|---|
| 1 | CuCl | 1.5 | 1.5 | DMSO | <10 |
| 2 | | 2 | 1.5 | DMSO | 66 |
| 3 | | 2 | 1 | DMSO | 59 |
| 4 | | 2 | 1 | DMF | <5 |
| 5 | CuI | 1.5 | 1.5 | DMSO | 18 |
| 6 | | 2 | 1.5 | DMSO | 37 |
| 7 | | 2 | 1 | DMSO | 29 |
| 8 | | 2 | 1 | DMF | <5 |
| 9 | CuBr | 1.5 | 1.5 | DMSO | 53 |
| 10 | | 2 | 1.5 | DMSO | 55 |
| 11 | | 2 | 1 | DMSO | 82 |
| 12 | | 2 | 1 | DMF | <5 |

[a]Yields determined by $^{19}F$ NMR vs Ph-$CF_3$ internal standard.

## Aryl Iodide Substrate Scope

With the optimal conditions in hand, we examined a small substrate scope for ttfet transfer to a series of substituted aryl iodides covering the span of electronic substituent effects. As shown in Table 3, all reactions furnished the desired product in moderate to very good yields. High yields were obtained with *ortho*-substituted substrates (**8b,c**), as observed by Grushin et al. for trifluoromethylations;[38] *para* substitution often (**8f,g**) but not generally (**8h,i**) gave less product. Electronic substituent effects do not appear dominant, with high yields obtained for electron-withdrawing (**8h,i**) as well as-donating substituents (**8b,c**).



https://doi.org/10.1021/acsorginorgau.4c00038
ACS Org. Inorg. Au 2024, 4, 628−639

**Table 3. Substrate Scope for −[CF(OCF$_3$)CF$_2$H] Transfer to Aryl Iodides**[a]

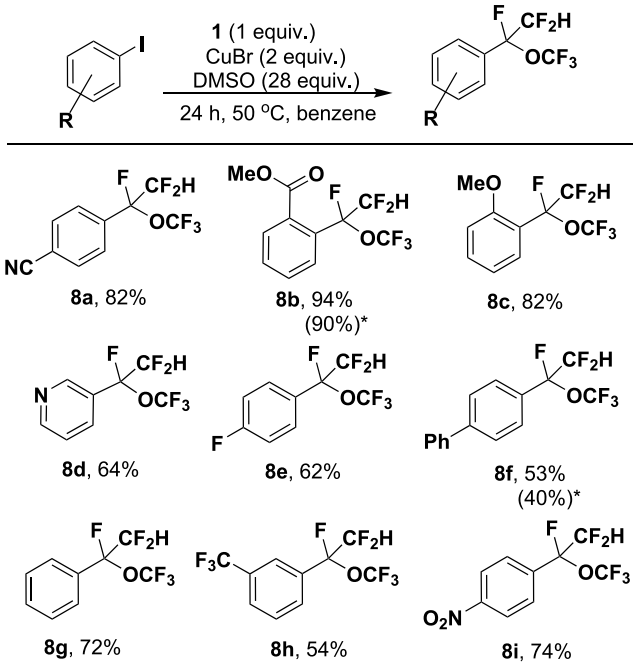


[a]Yields are determined by $^{19}$F NMR integrations vs Ph-CF$_3$ internal standard. Isolated yields from 0.3 mmol scale reactions are in brackets.

A subset of these substrates was chosen for scale-up and isolation. Compound **8b** was successfully purified via column chromatography, yielding 90%. Its structure was further validated through X-ray crystallography (Figure 4A). During the reaction of 3-iodopyridine with complex **1** to give **8d**, a significant amount of white solid precipitated. The solid was subsequently filtered, and its structure was determined using X-ray analysis, revealing a dinuclear pseudotetrahedral copper-(I) complex (**9**) with bridging bromides and each copper coordinated to both PPh$_3$ and iodopyridine ligands (Figure 4B).[41] This observation aligns well with the proposed role of CuBr as an effective trap for PPh$_3$ in this reaction system.

## Computational Insights into the Role of DMSO

The reaction of complex **1** with benzoyl chloride was computationally interrogated at the DFT level (TPSSh-D0/TZ//TPSSTPSS/DZ; see SI for further details) utilizing an approach previously employed in studying selective copper complex-catalyzed hydrodefluorination of fluoroalkenes.[42]

**Potential Energy Surface.** Modeling the effect of solvent by employing solvent corrections indicated only minimal (PCM:[43] 1.5 kcal/mol) or absent (SMD[44]) effects of increased solvent polarity with respect to gas phase calculations, which does not reflect experiment. Therefore, we decided to model solvent coordination explicitly—Scheme 3 depicts the Gibbs free energy surface with and without coordinated solvent molecule(s). Decoordination of one PPh$_3$ ligand (L) from **1** precedes oxidative addition of benzoyl chloride and is strongly endergonic (**LCu-R$_f$**: 18.5 kcal/mol) without coordinating solvents (black trace). The barrier for oxidative addition from **1** is sizable (**OxAd TS**: 21.2 kcal/mol), predominantly due to formation of the monoligated **LCu-R$_f$** complex. Formation of the square-planar, formally Cu(III), intermediate is endergonic (+12.2 kcal/mol). Rate limiting is the reductive elimination (**RedEl TS**: 25.7 kcal/mol) which is strongly exergonic (**L$_2$Cu-Cl** + **3a**: −23 kcal/mol). *β*-F elimination from the **LCu-R$_f$** complex to form **L$_2$CuF** and fluoroalkene is not competitive because it is endergonic (+2.6 kcal/mol); there is no obvious escape route, and the resulting olefin would only be reinserted under the experimental conditions. Coordination of two solvent molecules stabilizes the monophosphine complex; however, DMSO (**LCu(2DMSO)-R$_f$**: 2.2 kcal/mol, green trace) is much more effective than either acetone (12.7 kcal/mol) or acetonitrile (11.9 kcal/mol). The oxidative addition TS is stabilized by coordination of a single solvent molecule, with all three solvents showing similar stabilization ability (≈4 kcal/mol). However, of the three tested solvents, only DMSO stabilizes the square-pyramidal formal Cu(III)-intermediate and the **RedEl TS** strongly enough to overcome the entropic penalty for solvent coordination (**RedEl TS**: 21.1 kcal/mol). This barrier height is in line with the slow reaction observed experimentally. 5-coordinated Cu(III)-complexes have recently been isolated by Shen and co-workers.[45−47] In order to understand the effects that solvent coordination has on the

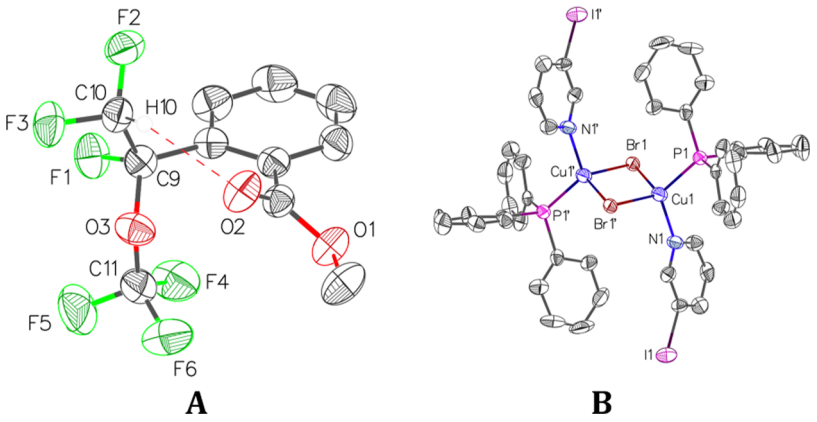


**Figure 4.** ORTEP representation of the molecular structures of **8b** (A) and **9** (B). Thermal ellipsoid probabilities are set to 50%, with hydrogen atoms omitted for clarity. Selected bond distances (Å) and angles (°) for **8b**: F1-C9 1.375(2) F2-C10 1.358(2) H10-C10 1.000 O3-C9 1.418(2) O3-C11 1.344(2) C9-C10 1.530(2) C9-O3-C11 121.7(1) C9-C10-H10 111.0 and for **9**: Cu1-Br1 2.515(1) Cu1-Br1′ 2.567(1) Cu1-P1 2.210(2) Cu1-N1 2.046(7) Cu1-Br1-Cu1′ 71.26(4) Br1-Cu1-P1 111.31(7) Br1-Cu1-N1 107.8(2) Br1-Cu1-Br1′ 108.74(5). Disorder of the OCF$_3$ group in **8b** is not shown, and all hydrogens except H10 are omitted for clarity. Dimer **9** is generated by symmetry around an inversion center; one cocrystallized molecule of benzene per Cu is omitted for clarity.



https://doi.org/10.1021/acsorginorgau.4c00038
ACS Org. Inorg. Au 2024, 4, 628−639

**Scheme 3. Potential Energy Surface for the Reaction of 1 with Benzoyl Chloride to Form 3a**[a]

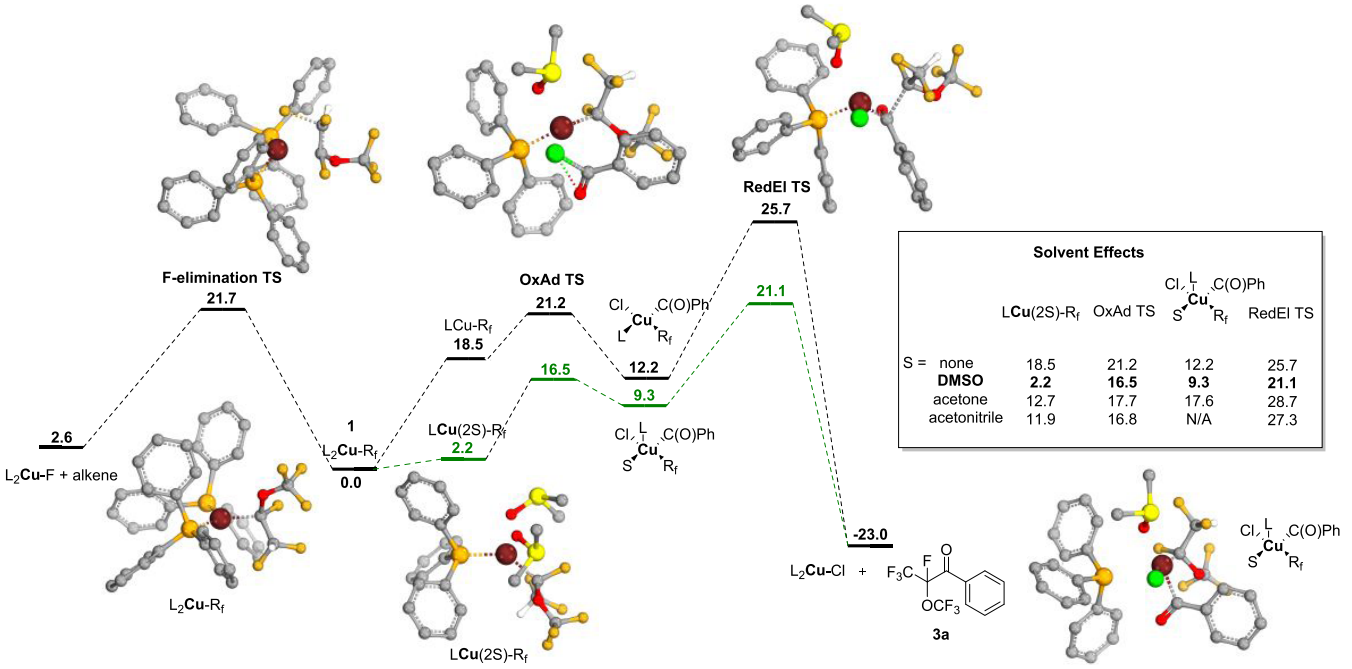


[a]Black trace without coordinated solvent, green trace with coordinated DMSO. Insert shows relative energies of key species for different solvents with respect to **1** ($L_2Cu\text{-}R_f$; $R_f = -[CF(OCF_3)CF_2H]$). $T$ = 298.15 K. Gibbs free energies in kcal/mol.

barrier heights and the stability of the intermediate it is instructive to analyze those species in more detail.

**Cu(III) or Cu(I)?** Snyder was the first to propose that the formal Cu(III) square-planar $[Cu(CF_3)_4]^-$ anion was really Cu(I).[48] He postulated an inverted ligand field, with the LUMO being primarily ligand centered and the $d_{x2-y2}$ orbital heavily occupied.

The ligand field inversion has been demonstrated spectroscopically by Lancaster et al.[49] They ascertained that "copper's limited capacity to be oxidized necessitates localization of electron hole character on the supporting ligands; consequently, the physical $d^8$ description for these formally Cu(III) species is inaccurate".[50] Overgaard has also confirmed the Cu(I) oxidation state by high-resolution X-ray single-crystal diffraction[51] but the debate continues.[52,53]

In the present case, several observations align with Snyder's findings. Although the intermediate is nearly perfectly square planar (depending on the level of theory) pointing to Cu(III), the frontier molecular orbitals are ligand-centered (Figure 5).

Natural Resonance Theory (NRT)[54] and Intrinsic Bond Orbital theory (IBO)[55−57] were used to further elucidate the nature of the intermediate. NRT allows us to determine the weights of contributing resonance structures to an idealized Lewis structure whereas Knizia's IBO method serves to further analyze the chemical bonding. A set of local orbitals (IBOs) is determined, exactly representing the computed Kohn−Sham wave function. Because IBOs intuitively depict occupied orbitals, they allow for a direct interpretation of chemical bonding. Charges are assigned to individual atoms without free parameters, electrons in doubly occupied IBOs are assigned proportionally to the individual atoms, allowing further quantitative interpretation of bonding.

NRT conforms with a Cu(I) species with an oxidized benzoyl ligand (Figure 5). IBO as well as natural bond orbital theory describe the Cu-P, Cu-Cl, and Cu-$R_f$ bonds as heavily polarized and ligand centered (>72% ligand contribution) while the Cu-$C_{aroyl}$ bond is heavily copper centered (75%). Wiberg bond indices[58] are <0.4, indicating substantial ionic contribution to the bond. Moreover, the Cu-P, Cu-Cl, and Cu-$R_f$ IBOs are partially localized on the aroyl fragment (5−9%), with the Cu-$R_f$ bond showing the largest contribution from $C_{aroyl}$. FMOs change only minimally when DMSO is coordinated; the bond composition of the Cu-Cl and Cu-$R_f$ bonds and the Cu-$C_{aroyl}$ change only minimally. The apical Cu-P bond is very long (3.076 Å). NRT now conforms more with Cu(III) species, however, with partial Cu(I) character (22.4%). The effective oxidation state of copper computed with IBOview according to the formalism by Ramos-Cordoba, Postils, and Salvador is in both cases +1.[59]

The rate limiting reductive elimination is concerted but decidedly asynchronous. In fact, in the solventless system, the Cu-$C_{aroyl}$ bond length is even shorter in the TS than it is in the intermediate (by 0.005 Å, Figure 6) and only minimally elongated in the DMSO case. Contrarily, the Cu-$R_f$ bond is elongated by 0.33 Å (no DMSO) and 0.41 Å (DMSO). Wiberg bond indices reflect these changes, with the Cu-$C_{aroyl}$ bond order changing only minimally while the one for the Cu-$R_f$ bond decreases from around 0.4 to around 0.15. Minimal changes occur in the Cu-$C_{aroyl}$ bond composition while the electron density of the forming C-C bond stems mostly from the $R_f$ fragment (approximately 2:1). Figure 7 depicts the electron flow along the reaction coordinate in the two IBOs with the largest changes along the reaction pathway, emphasizing the asynchronicity of the elimination (see MP4 videos in SI).

**Consequences of the Inverted Ligand Field and Solvent Stabilization.** Regardless of whether one sees the intermediates as Cu(III) or Cu(I), a picture emerges of a species in which the Cu-$R_f$ bond is heavily concentrated on the ligand, while the Cu-$C_{aroyl}$ bond is more concentrated on the


https://doi.org/10.1021/acsorginorgau.4c00038
ACS Org. Inorg. Au 2024, 4, 628−639

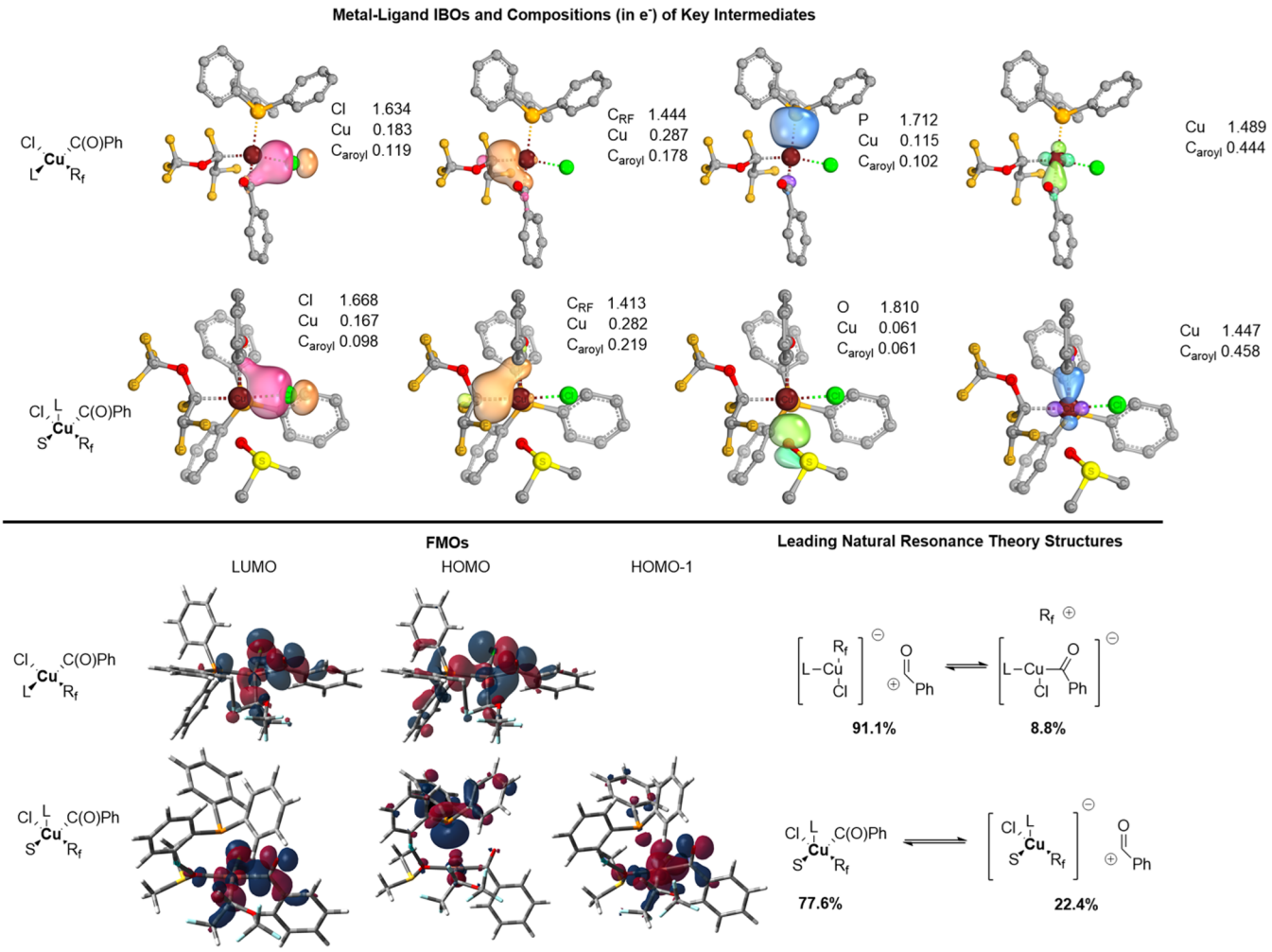


**Figure 5.** Metal−ligand IBOs, frontier molecular orbitals and NRT structures for the key intermediates. $R_f = -[CF(OCF_3)CF_2H]$.

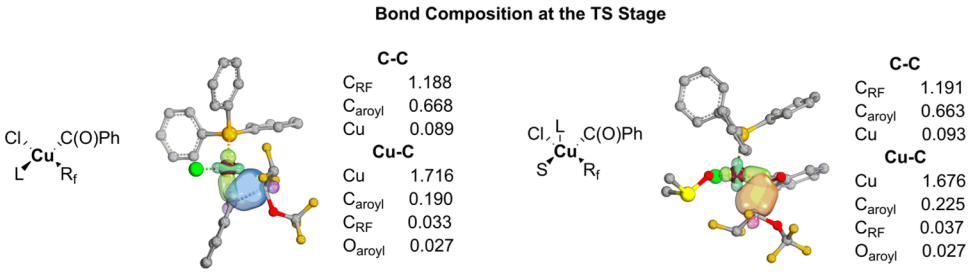


**Key Metric Parameters, Charges, WBI**

| | Bond Lengths | | | | IBO Charges) | | | | WBI | | |
|---|---|---|---|---|---|---|---|---|---|---|---|
| | Cu-$C_{RF}$ | Cu-$C_{aroyl}$ | $C_{RF}$-$C_{aroyl}$ | Cu-P | Cu | $C_{aroyl}$ | $C_{RF}$ | $O_{aroyl}$ | $C_{RF}$-$C_{aroyl}$ | Cu-$C_{RF}$ | Cu-$C_{aroyl}$ |
| | intermediate | | | | | | | | | | |
| none | 1.990 | 1.970 | 2.818 | 2.401 | 0.888 | 0.150 | 0.062 | -0.289 | - | 0.375 | 0.397 |
| DMSO | 1.988 | 1.947 | 2.803 | 3.076 | 0.947 | 0.163 | 0.085 | -0.284 | - | 0.382 | 0.463 |
| | TS | | | | | | | | | | |
| none | 2.327 | 1.965 | 2.094 | 2.326 | 0.788 | 0.191 | 0.213 | -0.336 | 0.463 | 0.145 | 0.316 |
| DMSO | 2.401 | 1.997 | 2.093 | 2.348 | 0.838 | 0.167 | 0.215 | -0.346 | 0.448 | 0.149 | 0.347 |

**Figure 6.** IBO bond composition at the TS stage, key metric parameters, charges and WBIs. H atoms omitted for clarity.

metal. This biases the complex for an easy reductive elimination more reminiscent of nucleophilic attack of the $R_f$ group on the aroyl fragment than traditional concerted reductive elimination mechanisms. In essence, this resembles acid−base chemistry. These findings align with Lancaster's



https://doi.org/10.1021/acsorginorgau.4c00038
ACS Org. Inorg. Au 2024, 4, 628−639

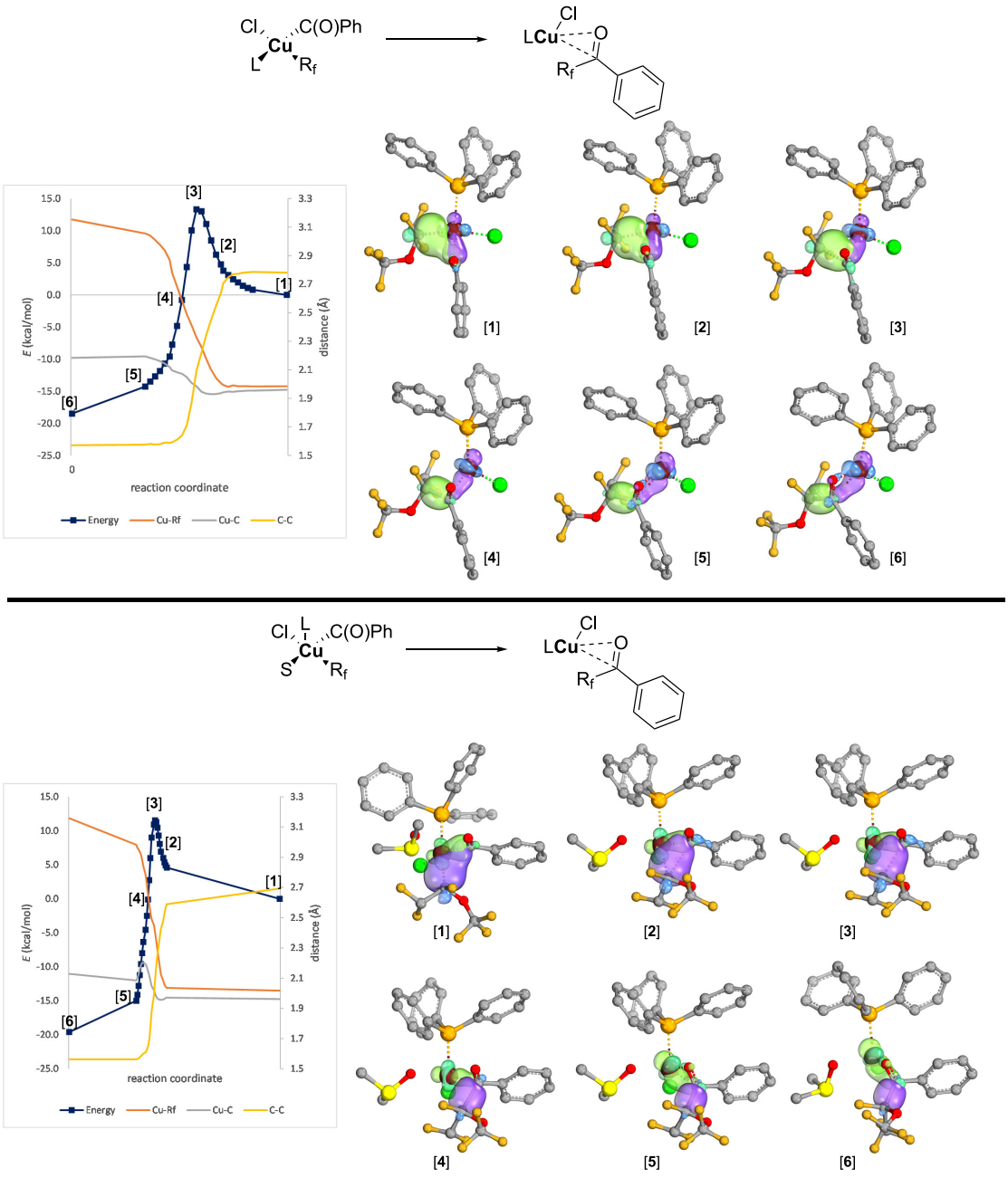


**Figure 7.** Electron flow along the intrinsic reaction coordinate (IRC) during reductive elimination. Hydrogen atoms omitted for clarity. The two IBOs with the largest changes along the reaction pathway are visualized.

analysis of reductive elimination[50] in $[Cu(benzyl)(CF_3)_3]^-$, and Klein and Knizia's findings[60] for Sanford's Ni-system.[61]

Square-pyramidal Cu-species like the DMSO-stabilized one here are heavily crowded, as emphasized by the long Cu-P in the intermediate (3.076 Å vs 2.401 Å in the square-planar species). DMSO, with its javelin-shaped O═S unit, develops steric bulk further away from the central metal than, for example, acetone. Furthermore, its strong negative point charge stabilizes the charge transfer during elimination. N-donors like acetonitrile, on the other hand, seem incapable of stabilizing such species sufficiently.

## CONCLUSIONS

The work described herein builds on our previous results accessing novel $R_f$ groups (*i.e.*, hfip,[33] $CF_2CF_2H$,[40,62] and $CFClCF_2H$[63]) via insertion of fluoroalkenes into Cu-H and Cu-F bonds. Although the $R_f$ transfers described herein are stoichiometric in copper, this protocol has proven valuable for late stage fluoroalkylation in the discovery phase of pharmaceutical and agrochemical research as evidenced by the commercialization of $CuCF_3(phen)$.[31] In contrast to Cu-hfip transfer that proceeded efficiently in DMF,[33] ttfet transfer is facilitated by DMSO, albeit as a *ligand* since complex **1** eventually decomposes in DMSO solvent. For ttfet transfer to aroyl chlorides, computational analysis revealed an inverted ligand field in the formal Cu(III) intermediate and a polarized $Cu\text{-}C_{aroyl}$ bond. The asynchronous transition state resembles nucleophilic attack of the $R_f$ group on the $\delta^+$ carbonyl carbon. Moreover, evidence was presented for $PPh_3$ oxidation, suggesting an additional role for DMSO in alleviating


https://doi.org/10.1021/acsorginorgau.4c00038
ACS Org. Inorg. Au 2024, 4, 628−639

phosphine binding pre-equilibria that could hinder the rate-determining reductive elimination step. Unfortunately, the aroyl-ttfet ketone products are less thermally stable than those containing $C_2F_5$[30] or hfip[33] groups.

For $R_f$ transfer from Cu to aryl iodides, oxidative addition is usually the rate-determining step which we showed previously to be hindered by ligand binding pre-equilibria.[62] In this work we show that addition of CuBr to sequester $PPh_3$, combined with DMSO as a ligand, allow for the successful transfer of the bulky ttfet group to aryl iodides. These methodologies thus introduce geminal $-OCF_3$ and $-CF_2H$ groups in a single transformation, enabling access to a bulky $R_f$ group that includes a hydrogen-bond donor.

## EXPERIMENTAL SECTION

### General Procedures

Experiments were conducted under nitrogen, using Schlenk techniques or an MBraun glovebox. All reactions were heated using an aluminum bead (Lab Armor) bath. Solvents were deoxygenated by purging with nitrogen. Tetrahydrofuran (thf), acetonitrile (MeCN), diethyl ether ($Et_2O$), hexanes and toluene were dried on columns of activated alumina using a J. C. Meyer (formerly Glass Contour) solvent purification system. 1,2-Dimethoxyethane (dme), cyclopentyl methyl ether (cpme) and benzene-$d_6$ ($C_6D_6$) were dried by stirring over activated alumina (ca. 10 wt. %) overnight, followed by filtration. All solvents were stored over activated (heated at ca. 250 °C for > 10 h under vacuum) 4 Å molecular sieves. Glassware was oven-dried at 120 °C for >2 h. The following chemicals were obtained commercially, as indicated: perfluoro(methyl vinyl ether) (PMVE, Synquest), pentane (Sigma-Aldrich, anhydrous, >99%), benzene (Sigma-Aldrich, anhydrous, 99.8%), cyclopentyl methyl ether (Sigma-Aldrich, anhydrous, >99%), *N*,*N*-dimethylformamide (Sigma-Aldrich, anhydrous, 99.8%), *N*,*N*-dimethylacetamide (Sigma-Aldrich, anhydrous, >99%), dimethylsulfoxide (DMSO, Alfa Aesar anhydrous, 99.8%), trifluorotoluene (Sigma-Aldrich, anhydrous, >99%), iodobenzene (Alfa Aesar, 98%), all other aryl iodides (Sigma-Aldrich), all acid chlorides (Sigma-Aldrich), 1,10-phenanthroline (phen, Sigma-Aldrich), 4,4′-dichloro-2,2′-bipyridine (bipy-$Cl_2$, Sigma-Aldrich), 2,9-dimethy-1,10-phenanthroline (dmphen, Sigma-Aldrich), triphenylphosphine ($PPh_3$, Oakwood Chemicals, 99%), methyldiphenylphosphine ($PMePh_2$, Acros Organics, 99%), tetramethyldisiloxane (TMDSO, Sigma-Aldrich, 97%), copper bromide (Sigma-Aldrich, 98%). The following chemicals were synthesized as previously reported: hexahydro-1,3-bis(2,4,6-trimethylphenyl)-1,3-diazepin-2-ylidene (7-dipp),[64] 1,3-bis(2,3,6-trimethylphenyl)-imidazol-2-ylidene (Imes)[65] and $[CuH(PPh_3)]_6$.[66] Electrospray ionization mass spectral data were collected using an Applied Biosystem API2000 triple quadrupole mass spectrometer. For electron impact (EI), solid samples were prepared by drying products under vacuum, and spectra obtained using a Kratos Concept S1 instrument (hres 7000−10,000). GC-MS analyses were performed on an Agilent Technologies 6890N GC system equipped with a 5973 network mass selective detector. NMR spectra $^1H$, $^{19}F$, $^{31}P\{^1H\}$, and $^{13}C\{^1H\}$ were recorded on a 300 MHz Bruker Avance instrument at room temperature (21−23 °C) unless stated otherwise. $^{13}C$ NMR spectra were referenced to solvent resonances and $^1H$ NMR spectra were referenced to residual proton peaks associated with the deuterated solvents ($C_6D_6$: 7.16). $^{31}P\{^1H\}$ NMR data were referenced to external $H_3PO_4$ (85% aqueous solution), set to 0.0 ppm. $^{19}F$ NMR spectra were referenced to internal standard $\alpha,\alpha,\alpha$-trifluorotoluene ($CF_3Ph$) (unless stated otherwise) set to −63.5 ppm. Details of synthesis, characterization and Cu-mediated $R_f$ transfer are included in the SI.

### X-ray Crystallography

Crystallographic data collection and processing were performed at the X-ray Core Facility at the University of Ottawa. Crystals were mounted on MiTeGen sample holders using Parabar oil. Data were collected on a Bruker Smart Apex or Bruker Kappa Apex diffractometer equipped with an ApexII CCD detector and a sealed-tube Mo K source ($\lambda$ = 0.71073 Å). During collection, the crystal was cooled to 200 K. Raw data collection and integration were performed with the Apex3 software package from Bruker.[67] Initial unit cell parameters were determined from 36 data frames from selected $\omega$ scans. Semiempirical absorption corrections based on equivalent reflections were applied using SADABS or TWINABS.[68,69] Systematic absences in the diffraction data set and unit cell parameters were consistent with the space group determined via the XPREP program.[70] Hydrogen atoms on carbons were placed geometrically and refined using the riding model, all other hydrogen atoms were placed via the difference map and refined freely. Data collection and structure refinement details are provided in Tables S4 and S5.

Twinning in compound **5b** was identified using CELL_NOW.[71] Two twin components were integrated and absorption correction applied via TWINABS. Refinement of the twin fraction was included along with the general refinements using HKLF5 data.

### Computational Details

All geometries were fully optimized by using the Gaussian 16 software package.[72] The BOpt software package was employed for data collection.[73] Following a proposed protocol,[74] all relevant minima and transition states were fully optimized at the TPSSTPSS level[75] of theory employing correlation-consistent polarized valence double-$\zeta$ Dunning (DZ) basis sets with cc-pVDZ quality[76,77] from the EMSL basis set exchange library,[78] using a small core pseudopotential on Cu.[79] The density fitting approximation (Resolution of Identity, RI)[80−83] was used at the optimization stage and for single-point energy corrections. All calculations were performed at the standard Gaussian 16 SCF convergence criteria using an ultrafine grid [Scf = Tight and Int(Grid = ultrafine)]. The nature of each stationary point was checked with an analytical second-derivative calculation (no imaginary frequency for minima, exactly one imaginary frequency for transition states, corresponding to the reaction coordinate). The accuracy of TS was confirmed with IRC scans. Transition states were located using a suitable guess and the Berny algorithm (Opt = TS)[84] or a relaxed potential energy scan to arrive at a suitable transition-state guess, followed by a quasi-Newton or eigenvector-following algorithm to complete the optimization. Final single-point energies were calculated at the TPSSh level of theory[75] employing triple-$\zeta$ Dunning (TZ) basis sets (cc-pVTZ quality).[76] Solvent effects (DMSO, $\varepsilon$ = 46.826) were included with the polarizable continuum model approach (PCM) or the SMD solvation model where indicated.[43,44] Grimme dispersion corrections without damping (keyword -zero) were added at this stage using the standalone dftd3 program.[85,86] Enthalpies and Gibbs free energies were then obtained from TZ single-point energies and thermal corrections from the TPSSTPSS-(PCM)/cc-pVDZ-(PP) vibrational analyses; entropy corrections were scaled by a factor of 0.67 to account for decreased entropy in the condensed phase.[87−89] NBO 7.0 was used for NBO analysis.[90] IBOview was used for intrinsic bond orbital theory (IBO) calculations,[55−57] employing SP Molden output files from Gaussian (utilizing the following input: *#p gfinput IOP(6/7 = 3) tpssh/def2TZVP/auto pseudo = read denfit int = grid = ultrafine*).

## ASSOCIATED CONTENT

### Data Availability Statement

The data underlying this study are available in the published article and its Supporting Information.

### Supporting Information

The Supporting Information is available free of charge at https://pubs.acs.org/doi/10.1021/acsorginorgau.4c00038.

Experimental synthesis details, crystallographic information, DFT table, GC-mass spectra, and $^1H$, $^{19}F$, $^{13}C\{^1H\}$, and $^{31}P\{^1H\}$ NMR spectra (PDF)

Combined file for all computational structures (XYZ)

RedEl_NoDMSO (MP4)



https://doi.org/10.1021/acsorginorgau.4c00038
ACS Org. Inorg. Au 2024, 4, 628−639

RedEl_withDMSO (MP4)

### Accession Codes

CCDC 2285055−2285056, 2285058−2285059, and 2285224 contain the supplementary crystallographic data for this paper. These data can be obtained free of charge via www.ccdc.cam.ac.uk/data_request/cif, or by emailing data_request@ccdc.cam.ac.uk, or by contacting The Cambridge Crystallographic Data Centre, 12 Union Road, Cambridge CB2 1EZ, UK; fax: +44 1223 336033.

## AUTHOR INFORMATION


### Corresponding Authors

**Christian Ehm** − *Dipartimento di Scienze Chimiche, Universitàdi Napoli Federico II, Via Cintia 80126 Napoli, Italy;* orcid.org/0000-0002-2538-5141; Email: christian.ehm@unina.it.

**R. Tom Baker** − *Department of Chemistry and Biomolecular Sciences and Centre for Catalysis Research and Innovation, University of Ottawa, Ottawa, Ontario K1N 6N5, Canada;* orcid.org/0000-0002-1133-7149; Email: rbaker@uottawa.ca.

### Authors

**Behnaz Ghaffari** − *Department of Chemistry and Biomolecular Sciences and Centre for Catalysis Research and Innovation, University of Ottawa, Ottawa, Ontario K1N 6N5, Canada*

**Luana L. T. N. Porto** − *Department of Chemistry and Biomolecular Sciences and Centre for Catalysis Research and Innovation, University of Ottawa, Ottawa, Ontario K1N 6N5, Canada*

**Nicole Johnson** − *Department of Chemistry and Biomolecular Sciences and Centre for Catalysis Research and Innovation, University of Ottawa, Ottawa, Ontario K1N 6N5, Canada*

**Jeffrey S. Ovens** − *Faculty of Science, University of Ottawa, Ottawa, Ontario K1N 6N5, Canada*

Complete contact information is available at: https://pubs.acs.org/10.1021/acsorginorgau.4c00038


### Author Contributions

‖B.G. and L.L.T.N.P. contributed equally. All experimental work was conducted by B.G., L.L.T.N.P., and N.J. and X-ray diffraction studies by J.S.O. All computational work was performed by C.E. and the manuscript was written and SI assembled through contributions of all authors. All authors have given approval to the final version of this manuscript.

### Notes

The authors declare no competing financial interest.

## ACKNOWLEDGMENTS

R.T.B. thanks the Natural Sciences and Engineering Research Council (Canada; grant RGpin-2019-05958) and the Canada Research Chairs program for generous financial support and the University of Ottawa, Canada Foundation for Innovation and Ontario Ministry of Economic Development and Innovation for essential infrastructure. B.G. thanks MITACS and Arkema for a postdoctoral fellowship. N.J. gratefully acknowledges support from Canada's Inorganic Chemistry Exchange program and C.E. thanks Prof. Vincenzo Busico and Peter H. M. Budzelaar (University of Naples Federico II) for their generous donation of CPU time.

## REFERENCES


(1) Zhou, Y.; Wang, J.; Gu, Z.; Wang, S.; Zhu, W.; Acena, J. L.; Soloshonok, V. A.; Izawa, K.; Liu, H. Next generation of fluorine-containing pharmaceuticals, compounds currently in phase II−III clinical trials of major pharmaceutical companies: New structural trends and therapeutic areas. *Chem. Rev.* **2016**, *116*, 422−518.

(2) Ogawa, Y.; Tokunaga, E.; Kobayashi, O.; Hirai, K.; Shibata, N. Current contributions of organofluorine compounds to the agrochemical industry. *iScience* **2020**, *23*, No. 101467.

(3) Neumann, C. N.; Ritter, T. Late-stage fluorination: Fancy novelty or useful tool? *Angew. Chem., Int. Ed.* **2015**, *54*, 3216−3221.

(4) Szpera, R.; Moseley, D. F. J.; Smith, L. B.; Sterling, A. J.; Gouverneur, V. The fluorination of C−H bonds: Developments and perspectives. *Angew. Chem., Int. Ed.* **2019**, *58*, 14824−14848.

(5) Han, Z.-Z.; Zhang, C.-P. Fluorination and fluoroalkylation reactions mediated by hypervalent iodine reagents. *Adv. Synth. Catal.* **2020**, *362*, 4256−4292.

(6) Britton, R.; Gouverneur, V.; Lin, J.-H.; Meanwell, M.; Ni, C.; Pupo, G.; Xiao, J.-C.; Hu, J. Contemporary synthetic strategies in organofluorine chemistry. *Nat. Rev.* **2021**, *1*, No. 47.

(7) Barata-Vallejo, S.; Lantano, B.; Postigo, A. Recent advances in trifluoromethylation reactions with electrophilic trifluoromethylating reagents. *Chem.−Eur. J.* **2014**, *20*, 16806−16829.

(8) Li, G.-B.; Zhang, C.; Song, C.; Ma, Y.-D. Progress in copper-catalyzed trifluoromethylation. *Beilstein J. Org. Chem.* **2018**, *14*, 155−181.

(9) Xiao, H.; Zhang, Z.; Fang, Y.; Zhu, L.; Li, C. Radical trifluoromethylation. *Chem. Soc. Rev.* **2021**, *50*, 6308−6319.

(10) Ohashi, M.; Ishida, N.; Ando, K.; Hashimoto, Y.; Shigaki, A.; Kikushima, K.; Ogoshi, S. $Cu^{I}$-catalyzed pentafluoroethylation of aryl iodides in the presence of tetrafluoroethylene and cesium fluoride: Determining the route to the key pentafluoroethyl $Cu^{I}$ intermediate. *Chem.−Eur. J.* **2018**, *24*, 9794−9798.

(11) Xie, Q.; Li, L.; Zhu, Z.; Zhang, R.; Ni, C.; Hu, J. From C1 to C2: $TMSCF_3$ as a precursor for pentafluoroethylation. *Angew. Chem., Int. Ed.* **2018**, *57*, 13211−13215.

(12) Xie, Q.; Zhu, Z.; Li, L.; Ni, C.; Hu, J. Controllable double $CF_2$ insertion into $sp^2$ C-Cu bond using $TMSCF_3$: A facile access to tetrafluoroethylene-bridged structures. *Chem. Sci.* **2020**, *11*, 276−280.

(13) Landelle, G.; Panossian, A.; Leroux, F. R. Trifluoromethyl ethers and -thioethers as tools for medicinal chemistry and drug discovery. *Curr. Top. Med. Chem.* **2014**, *14*, 941−951.

(14) Lee, K. N.; Lee, J. W.; Nga, M.-Y. Recent development of catalytic trifluoromethoxylation reactions. *Tetrahedron* **2018**, *74*, 7127−7135.

(15) Deng, Z.; Zhao, M.; Wang, F.; Tang, P. Selective C-H trifluoromethoxylation of (hetero)arenes as limiting reagent. *Nat. Commun.* **2020**, *11*, No. 2569.

(16) Fier, P. S.; Hartwig, J. F. Copper-mediated difluoromethylation of aryl and vinyl iodides. *J. Am. Chem. Soc.* **2012**, *134*, 5524−5527.

(17) Sap, J. B. I.; Meyer, C. F.; Straathof, N. J. W.; Iwumene, N.; am Ende, C. W.; Trabanco, A. A.; Gouverneur, V. Late-stage difluoromethylation: Concepts, developments and perspective. *Chem. Soc. Rev.* **2021**, *50*, 8214−8247.

(18) Zhang, W.; Xiang, X.-X.; Chen, J.; Yang, C.; Pan, Y.-L.; Cheng, J.-P.; Meng, Q.; Li, X. Direct C−H difluoromethylation of heterocycles via organic photoredox catalysis. *Nat. Commun.* **2020**, *11*, No. 638.

(19) Doble, A. The pharmacology and mechanism of action of riluzole. *Neurology* **1996**, *47*, 233S−241S.

(20) Belinato, T. A.; Martins, A. J.; Lima, J. B. P.; de Lima-Camara, T. N.; Peixoto, A. A.; Valle, D. Effect of the chitin synthesis inhibitor triflumuron on the development, viability and reproduction of *Aedes aegypti*. *Mem. Inst. Oswaldo Cruz.* **2009**, *104*, 43−47.

(21) Rageot, D.; Bohnacker, T.; Melone, A.; Langlois, J.-B.; Borsari, C.; Hillmann, P.; Sele, A. M.; Beaufils, F.; Zvelebil, M.; Hebeisen, P.; Löscher, W.; Burke, J.; Fabbro, D.; Wymann, M. P. Discovery and Preclinical Characterization of 5-[4,6-Bis({3-oxa-8-azabicyclo[3.2.1]-octan-8-yl})-1,3,5-triazin-2-yl]-4-(difluoromethyl)pyridin-2-amine

(PQR620), a Highly Potent and Selective mTORC1/2 Inhibitor for Cancer and Neurological Disorders. *J. Med. Chem.* **2018**, *61*, 10084−10105.
(22) Liu, K.; Wen, Z.; Ma, Z.; Shao, W. Biological and molecular characterizations of fluxapyroxad-resistant isolates of *Botrytis cinerea*. *Phytopathol. Res.* **2022**, *4*, No. 2.
(23) Xing, L.; Blakemore, D. C.; Narayanan, A.; Unwalla, R.; Lovering, F.; Denny, R. A.; Zhou, H.; Bunnage, M. E. Fluorine in drug design: A case study with fluoroanisoles. *ChemMedChem* **2015**, *10*, 715−726.
(24) Abraham, M. H.; Abraham, R. J. A simple and facile NMR method for the determination of hydrogen bonding by amide N−H protons in protein models and other compounds. *New J. Chem.* **2017**, *41*, 6064−6066.
(25) Miele, M.; D'Orsi, R.; Sridharan, V.; Holzer, W.; Pace, V. Highly chemoselective difluoromethylative homologation of iso-(thio)cyanates: Expeditious access to unprecedented $\alpha,\alpha$-difluoro-(thio)amides. *Chem. Commun.* **2019**, *55*, 12960−12963.
(26) Berger, M.; Herszman, J. D.; Kurimoto, Y.; de Kruiff, G. H. M.; Schüll, A.; Ruf, S.; Waldvogel, S. R. Metal-free electrochemical fluorodecarboxylation of aryloxyacetic acids to fluoromethyl aryl ethers. *Chem. Sci.* **2020**, *11*, 6053−6057.
(27) Zhang, J.; Tang, X.; Ishaaya, I.; Cao, S.; Wu, J.; Yu, J.; Li, H.; Qian, X. Synthesis and insecticidal activity of heptafluoroisopropyl-containing benzoylphenylurea structures. *J. Agric. Food Chem.* **2010**, *58*, 2736−2740.
(28) Zhou, S.; Meng, X.; Jin, R.; Ma, Y.; Xie, Y.; Zhao, Y.; Song, H.; Xiong, L.; Li, Z. Synthesis, insecticidal activities and structure activity relationship study of dual chiral sulfilimines. *Mol. Diversity* **2017**, *21*, 915−923.
(29) Tomashenko, O. A.; Escudero-Adàn, E. C.; Belmonte, M. M.; Grushin, V. V. Simple, stable and easily accessible well-defined $CuCF_3$ aromatic trifluoromethylating agents. *Angew. Chem., Int. Ed.* **2011**, *50*, 7655−7659.
(30) Panferova, L. I.; Miloserdov, F. M.; Lishchynskyi, A.; Belmonte, M. M.; Benet-Bucholz, J.; Grushin, V. V. Well-defined $CuC_2F_5$ complexes and pentafluoroethylation of acid chlorides. *Angew. Chem., Int. Ed.* **2015**, *54*, 5218−5222.
(31) Morimoto, H.; Tsubogo, T.; Litvinas, N. D.; Hartwig, J. F. A broadly applicable copper reagent for trifluoromethylations and perfluoroalkylations of aryl iodides and bromides. *Angew. Chem., Int. Ed.* **2011**, *50*, 3793−3798.
(32) Kaplan, P. T.; Vicic, D. A. Versatile route to arylated fluoroalkyl bromide building blocks. *Org. Lett.* **2016**, *18*, 884−886.
(33) Andrella, N. O.; Liu, K.; Gabidullin, B. M.; Vasiliu, M.; Dixon, D. A.; Baker, R. T. Metal heptafluoroisopropyl (M-hfip) complexes for use as hfip transfer agents. *Organometallics* **2018**, *37*, 422−432.
(34) For synthesis of silver hfip complexes from Ag-F and HFP see: Miller, W. T., Jr.; Burnard, R. J. Perfluoroalkylsilver compounds. *J. Am. Chem. Soc.* **1968**, *90*, 7367.
(35) For a similar result with difluoromethylations, see: Xu, L.; Vicic, D. A. Direct difluoromethylation of aryl halides via base metal catalysis at room temperature. *J. Am. Chem. Soc.* **2016**, *138*, 2536−2539.
(36) Löw, S.; Becker, J.; Würtele, C.; Miska, A.; Kleeberg, C.; Behrens, U.; Walter, O.; Schindler, S. Reactions of copper(II) chloride in solution: Facile formation of tetranuclear copper clusters and other complexes that are relevant to catalytic redox processes. *Chem.−Eur. J.* **2013**, *19*, 5342−5353.
(37) Kalkman, E. D.; Mormino, M. G.; Hartwig, J. F. Unusual electronic effects of ancillary ligands on the perfluoroalkylation of aryl iodides and bromides mediated by copper(I) pentafluoroethyl complexes of substituted bipyridines. *J. Am. Chem. Soc.* **2019**, *141*, 19458−19465.
(38) Lishchynskyi, A.; Novikov, M. A.; Martin, E.; Escudero-Adàn, E. C.; Novàk, P.; Grushin, V. V. Trifluoromethylation of aryl and heteroaryl halides with fluoroform-derived $CuCF_3$: Scope, limitations and mechanistic features. *J. Org. Chem.* **2013**, *78*, 11126−11146.
(39) Mestre, J.; Castillón, S.; Boutureira, O. "Ligandless" pentafluoroethylation of unactivated (hetero)aryl and alkenyl halides enabled by the controlled self-condensation of $TMSCF_3$-derived $CuCF_3$. *J. Org. Chem.* **2019**, *84*, 15087−15097.
(40) Segovia, C. M.; Porto, L. L. T. N.; Ahmad, A.; Casasús, P.; Bascuas, I.; Mestre, J.; Bernús, M.; Castillón, S.; Baker, R. T.; Boutureira, O. Tetrafluoroethylation of electron-rich alkenyl iodides enabled by *in situ* generation of solvent-stabilized 'ligandless' $CuCF_2CF_2H$". *Adv. Synth. Catal.* **2024**, *366*, 2684−2690.
(41) For a similar structure, $[Cu(\mu\text{-}I)(PPh_3)(3\text{-bromo-pyridine})]_2$, see: Liu, W.; Zhu, K.; Teat, S. J.; Delbert, B. J.; Yuan, W.; Li, J. J. A mechanochemical route toward the rational, systematic, and cost-effective green synthesis of strongly luminescent copper iodide based hybrid phosphors. *J. Mater. Chem. C* **2017**, *5* (24), 5962−5969.
(42) Andrella, N. O.; Xu, N.; Gabidullin, B. M.; Ehm, C.; Baker, R. T. Selective copper-complex catalyzed hydrodefluorination of fluoroalkenes and allyl fluorides: A tale of two mechanisms. *J. Am. Chem. Soc.* **2019**, *141*, 11506−11521.
(43) Tomasi, J. Thirty years of continuum solvation chemistry: A review, and prospects for the near future. *Theor. Chem. Acc.* **2004**, *112*, 184−203.
(44) Marenich, A. V.; Cramer, C. J.; Truhlar, D. G. Universal solvation model based on solute electron density and on a continuum model of the solvent defined by the bulk dielectric constant and atomic surface tensions. *J. Phys. Chem. B* **2009**, *113*, 6378−6396.
(45) Lu, Z.; Liu, H.; Liu, S.; Leng, X.; Lan, Y.; Shen, Q. A Key Intermediate in copper-mediated arene trifluoromethylation, $[nBu_4N][Cu(Ar)(CF_3)_3]$: Synthesis, characterization, and $C(sp^2)-CF_3$ reductive elimination. *Angew. Chem., Int. Ed.* **2019**, *58*, 8510−8514.
(46) Liu, H.; Shen, Q. Bistrifluoromethylated organocuprate $[Ph_4P]^+[Cu(CF_3)_2]^-$: Synthesis, characterization and its application for trifluoromethylation of activated heteroaryl bromides, chlorides and iodides. *Org. Chem. Front.* **2019**, *6*, 2324−2328.
(47) Wang, G.; Li, M.; Leng, X.; Xue, X.; Shen, Q. Neutral five-coordinate arylated copper(III) complex: Key intermediate in copper-mediated arene trifluoromethylation. *Chin. J. Chem.* **2022**, *40*, 1924−1930.
(48) Snyder, J. P. Elusiveness of Cu(III) complexation; preference for trifluoromethyl oxidation in the formation of $[Cu^I(CF_3)_4]^-$ salts. *Angew. Chem., Int. Ed.* **1995**, *34*, 80−81.
(49) Walroth, R. C.; Lukens, J. T.; MacMillan, S. N.; Finkelstein, K. D.; Lancaster, K. M. Spectroscopic evidence for a $3d^{10}$ ground State electronic configuration and ligand field inversion in $[Cu(CF_3)_4]^-$. *J. Am. Chem. Soc.* **2016**, *138*, 1922−1931.
(50) DiMucci, I. M.; Lukens, J. T.; Chatterjee, S.; Carsch, K. M.; Titus, C. J.; Lee, S. J.; Nordlund, D.; Betley, T. A.; MacMillan, S. M.; Lancaster, K. M. The myth of $d^8$ copper(III). *J. Am. Chem. Soc.* **2019**, *141*, 18508−18520.
(51) Gao, C.; Macetti, G.; Overgaard, J. Experimental X-ray electron density study of atomic charges, oxidation states, and inverted ligand field in $[Cu(CF_3)_4]^-$. *Inorg. Chem.* **2019**, *58*, 2133−2139.
(52) Geoghegan, B. L.; Liu, Y.; Peredkov, S.; Dechert, S.; Meyer, F.; DeBeer, S.; Cutsail, G. E., III Combining valence-to-core X-ray emission and Cu K-edge X-ray absorption spectroscopies to experimentally assess oxidation state in organometallic Cu(I)/(II)/(III) complexes. *J. Am. Chem. Soc.* **2022**, *144*, 2520−2534.
(53) Hoffmann, R.; Alvarez, S.; Mealli, C.; Falceto, A.; Cahill, T. J.; Zeng, T.; Manca, G. From widely accepted concepts in coordination chemistry to inverted ligand fields. *Chem. Rev.* **2016**, *116*, 8173−8192.
(54) Glendening, E. D.; Weinhold, F. Natural resonance theory: I. General formalism. *J. Comput. Chem.* **1998**, *19*, 593−609.
(55) Knizia, G. Intrinsic atomic orbitals: An unbiased bridge between quantum theory and chemical concepts. *J. Chem. Theory Comput.* **2013**, *9*, 4834−4843.
(56) Knizia, G.; Klein, J. E. M. N. Electron flow in reaction mechanisms-revealed from first principles. *Angew. Chem., Int. Ed.* **2015**, *54*, 5518−5522.


https://doi.org/10.1021/acsorginorgau.4c00038
*ACS Org. Inorg. Au* 2024, 4, 628−639

(57) Nunes dos Santos Comprido, L.; Klein, J. E. M. N.; Knizia, G.; Kästner, J.; Hashmi, A. S. K. The stabilizing effects in gold carbene complexes. *Angew. Chem., Int. Ed.* **2015**, *54*, 10336−10340.
(58) Wiberg, K. B. Application of the Pople-Santry-Segal CNDO method to the cyclopropylcarbinyl and cyclobutyl cation and to bicyclobutane. *Tetrahedron* **1968**, *24*, 1083−1096.
(59) Ramos-Cordoba, E.; Postils, V.; Salvador, P. Oxidation states from wave function analysis. *J. Chem. Theory Comput.* **2015**, *11*, 1501−1508.
(60) Steen, J. S.; Knizia, G.; Klein, J. E. M. N. σ-Noninnocence: Masked phenyl-cation transfer at formal $Ni^{IV}$. *Angew. Chem., Int. Ed.* **2019**, *58*, 13133−13139.
(61) Bour, J. R.; Camasso, N. M.; Sanford, M. S. Oxidation of Ni(II) to Ni(IV) with aryl electrophiles enables Ni-mediated aryl-$CF_3$ coupling. *J. Am. Chem. Soc.* **2015**, *137*, 8034−8037.
(62) Andrella, N. O. Synthesis of organo-fluorine compounds by metal complex-mediated and -catalyzed transformation of fluoroalkenes and fluoroarenes; University of Ottawa, PhD thesis, 2018.
(63) Porto, L. L. T. N.; Seifi, M.; Johnson, N.; Baker, R. T. Generation of copper fluoroalkyl complexes ($CuR^FL_n$) from chlorotrifluoroethylene and -$R^F$ transfer to aroyl chlorides. *Can. J. Chem.* **2023**, *101*, 470−476.
(64) Rzhevskiy, S. A.; Topchiy, M. A.; Lyssenko, K. A.; Philippova, A. N.; Belaya, M. A.; Ageshina, A. A.; Bermeshev, M. V.; Nechaev, M. S.; Asachenko, A. F. New expanded-ring NHC platinum(0) complexes: Synthesis, structure and highly efficient diboration of terminal alkenes. *J. Organomet. Chem.* **2020**, *912*, No. 121140.
(65) Arduengo, A. J., III.; Krafczyk, R.; Schmutzler, R.; Craig, H. A.; Goerlich, J. R.; Marshall, W. J.; Unversagt, M. Imidazolylidenes, imidazolinylidenes and imidazolines. *Tetrahedron* **1999**, *55*, 14523−14534.
(66) Lee, D.-W.; Yun, J. Direct synthesis of Stryker's reagent from a Cu(II) salt. *Tetrahedron Lett.* **2005**, *46*, 2037−2039.
(67) Bruker. *APEX3 Crystallography Software Suite*; Bruker AXS Inc.: Madison, WI, USA, 2016.
(68) Sheldrick, G. M. *SADABS*, Version 2008/1, 2008. Bruker AXS Inc., Germany.
(69) Sheldrick, G. M. *APEX-II, SAINT-Plus and TWINABS*, 2014, Bruker-Nonius AXS Inc., Madison.
(70) Sheldrick, G. M. A short history of SHELX. *Acta Crystallogr., Sect. A: Found. Crystallogr.* **2008**, *64*, 112.
(71) Sheldrick, G. M. CELL_NOW. *Acta Crystallogr., Sect. B*, **2004**.
(72) Frisch, M. J.; Trucks, G. W.; Schlegel, H. B.; Scuseria, G. E.; Robb, M. A.; Cheeseman, J. R.; Scalmani, G.; Barone, V.; Petersson, G. A.; Nakatsuji, H.; Li, X.; Caricato, M.; Marenich, A. V.; Bloino, J.; Janesko, B. G.; Gomperts, R.; Mennucci, B.; Hratchian, H. P.; Ortiz, J. V.; Izmaylov, A. F.; Sonnenberg, J. L.; Williams-Young, D.; Ding, F.; Lipparini, F.; Egidi, F.; Goings, J.; Peng, B.; Petrone, A.; Henderson, T.; Ranasinghe, D.; Zakrzewski, V. G.; Gao, J.; Rega, N.; Zheng, G.; Liang, W.; Hada, M.; Ehara, M.; Toyota, K.; Fukuda, R.; Hasegawa, J.; Ishida, M.; Nakajima, T.; Honda, Y.; Kitao, O.; Nakai, H.; Vreven, T.; Throssell, K.; Montgomery, J. A., Jr.; Peralta, J. E.; Ogliaro, F.; Bearpark, M. J.; Heyd, J. J.; Brothers, E. N.; Kudin, K. N.; Staroverov, V. N.; Keith, T. A.; Kobayashi, R.; Normand, J.; Raghavachari, K.; Rendell, A. P.; Burant, J. C.; Iyengar, S. S.; Tomasi, J.; Cossi, M.; Millam, J. M.; Klene, M.; Adamo, C.; Cammi, R.; Ochterski, J. W.; Martin, R. L.; Morokuma, K.; Farkas, O.; Foresman, J. B.; Fox, D. J. *Gaussian 16, revision A.03*; Gaussian, Inc.: Wallingford, CT, 2016.
(73) Budzelaar, P. H. M. Geometry optimization using generalized, chemically meaningful constraints. *J. Comput. Chem.* **2007**, *28*, 2226−2236.
(74) Ehm, C.; Budzelaar, P. H. M.; Busico, V. Calculating accurate barriers for olefin insertion and related reactions. *J. Organomet. Chem.* **2015**, *775*, 39−49.
(75) Tao, J.; Perdew, J. P.; Staroverov, V. N.; Scuseria, G. E. Climbing the density functional ladder: Nonempirical meta-generalized gradient approximation designed for molecules and solids. *Phys. Rev. Lett.* **2003**, *91*, No. 146401.
(76) Balabanov, N. B.; Peterson, K. A. Systematically convergent basis sets for transition metals. I. All-electron correlation consistent basis sets for the 3d elements Sc−Zn. *J. Chem. Phys.* **2005**, *123*, No. 064107.
(77) Balabanov, N. B.; Peterson, K. A. Basis set limit electronic excitation energies, ionization potentials, and electron affinities for the 3d transition metal atoms: Coupled cluster and multireference methods. *J. Chem. Phys.* **2006**, *125*, No. 074110.
(78) Pritchard, B. P.; Altarawy, D.; Didier, B.; Gibson, T. D.; Windus, T. L. New basis set exchange: An open, up-to-date resource for the molecular sciences community. *J. Chem. Inf. Model.* **2019**, *59*, 4814−4820.
(79) Schwerdtfeger, P. The pseudopotential approximation in electronic structure theory. *ChemPhysChem* **2011**, *12*, 3143−3155.
(80) Whitten, J. L. Coulombic potential energy integrals and approximations. *J. Chem. Phys.* **1973**, *58*, 4496.
(81) Baerends, E. J.; Ellis, D. E.; Ros, P. Self-consistent molecular Hartree—Fock—Slater calculations I. The computational procedure. *Chem. Phys.* **1973**, *2*, 41−51.
(82) Feyereisen, M.; Fitzgerald, G.; Komornicki, A. Use of approximate integrals in ab initio theory. An application in MP2 energy calculations. *Chem. Phys. Lett.* **1993**, *208*, 359−363.
(83) Vahtras, O.; Almlöf, J.; Feyereisen, M. W. Integral approximations for LCAO-SCF calculations. *Chem. Phys. Lett.* **1993**, *213*, 514−518.
(84) The Berny algorithm was never fully published, see the Gaussian documentation for details.
(85) Grimme, S. Density functional theory with London dispersion corrections. *Wiley Interdiscip. Rev.: Comput. Mol. Sci.* **2011**, *1*, 211−228.
(86) Grimme, S.; Ehrlich, S.; Goerigk, L. Effect of the damping function in dispersion corrected density functional *Theory*. *J. Comput. Chem.* **2011**, *32*, 1456−1465.
(87) Tobisch, S.; Ziegler, T. Catalytic oligomerization of ethylene to higher linear α-olefins promoted by the cationic group 4 $[(\eta^5\text{-Cp-}(CMe_2\text{-bridge})\text{-Ph})M^{II}(\text{ethylene})_2]^+$ (M = Ti, Zr, Hf) active catalysts: A density functional investigation of the influence of the metal on the catalytic activity and selectivity. *J. Am. Chem. Soc.* **2004**, *126*, 9059−9071.
(88) Zaccaria, F.; Ehm, C.; Budzelaar, P. H. M.; Busico, V. Accurate prediction of copolymerization statistics in molecular olefin polymerization catalysis: The role of entropic, electronic, and steric effects in catalyst comonomer affinity. *ACS Catal.* **2017**, *7*, 1512−1519.
(89) Zaccaria, F.; Cipullo, R.; Budzelaar, P. H. M.; Busico, V.; Ehm, C. Backbone rearrangement during olefin capture as the rate limiting step in molecular olefin polymerization catalysis and its effect on comonomer affinity. *J. Polym. Sci., Part A: Polym. Chem.* **2017**, *55*, 2807−2814.
(90) NBO 7.0; Glendening, E. D.; Badenhoop, J. K.; Reed, A. E.; Carpenter, J. E.; Bohmann, J. A.; Morales, C. M.; Karafiloglou, P.; Landis, C. R.; Weinhold, F.. *Theoretical Chemistry Institute*; University of Wisconsin: Madison, 2018.


https://doi.org/10.1021/acsorginorgau.4c00038
ACS Org. Inorg. Au 2024, 4, 628−639